Published in final edited form as:
Macromolecules. 2012 October 23; 45(20): 8373–8381. doi:10.1021/ma300981r.

How Bacteria Adhere to Brushy PEG Surfaces: Clinging to Flaws and Compressing the Brush

S. Gon[1], **Kushi-Nidhi Kumar**[2], **Klaus Nüsslein**[2], and **Maria M. Santore**[3]

[1]Department of Chemical Engineering, Univeristy of Massachusetts Amherst, MA 01003

[2]Department of Microbiology, Univeristy of Massachusetts Amherst, MA 01003

[3]Department of Polymer Science and Engineering, Univeristy of Massachusetts Amherst, MA 01003

Abstract

This study examined the compression of solvated polymer brushes on bioengineered surfaces during the initial stages of *Staphylococcus Aureus* (*S. aureus*) adhesion from gentle flow. A series of PEG [poly(ethylene glycol)] brushes, 7 to 17 nm in height and completely non-adhesive to proteins and bacteria, were modified by the incorporation of sparse isolated ~10 nm cationic polymer "patches" at their bases. These nanoscale regions, which lacked PEG tethers, were electrostatically attractive towards negative bacteria or proteins. *S. aureus* drawn to the interface by multiple adhesive patches compressed the PEG brush in the remaining contact region. The observed onset of bacterial or fibrinogen capture with increases in patch content was compared with calculations. Balancing the attraction energy (proportional to the number of patches engaging a bacterium during capture) against steric forces (calculated using the Alexander-DeGennes treatment) provided perspective on the brush compression. The results were consistent with a bacteria-surface gap on the order of the Debye length in these studies. In this limit of strong brush compression, structural features (height, persistence length) of the brush were unimportant so that osmotic pressure dominated the steric repulsion. Thus, the dominant factor for bacterial repulsion was the mass of PEG in the brush. This result explains empirical reports in the literature that identify the total PEG content of a brush as a criteria for prevention of bioadhesion, independent of tether length and spacing, within a reasonable range for those parameters. Bacterial capture was also compared to that of protein capture. It was found, surprisingly, that the patchy brushes were more protein-than bacteria-resistant. *S. aureus* adhesion driven by patches within otherwise protein-resistant PEG brushes was explained by the bacteria's greater tendency to compress large areas of brush to interact with many patches. By contrast, proteins are thought to penetrate the brush at a few sites of PEO-free patches. The finding provides a mechanism for the literature reports that *in-vitro* protein resistance is a poor predictor of *in-vitro* implant failure related to cell-surface adhesion.

Keywords

PEG brush; PEGylated surface; protein adsorption; polymer brush compression; steric repulsion; PEG surface loading; bacteria adhesion; brush compression; brush penetration; steric repulsion

Introduction

Solvated polymer brushes, for instance tethered polyethylene glycol (PEG), are commonly placed on surfaces to inhibit bio-fouling by proteins and cells.[1,2] Key to the bioadhesion-resistance of these interfaces (beyond choosing a polymer chemistry that is fundamentally protein-repellant: neutral, hydrophilic, well-hydrated, and hydrogen bond accepting[3]) is the

physical design of the brush. Its height must exceed the range of electrostatic[4] and van der Waals attractions[5,6] and its density must be sufficient to avoid penetration by small proteins.[6,7] Classic in the literature, surface forces experiments on solvated brushes generally confirm the expected force-distance profiles that tend to be strongly repulsive and long in range,[8-15] while atomic force microscopy indicates less repulsion due to tip penetration into the brush.[9] A recent study of PEG brushes with colloidal force microscopy demonstrated the relative ranges of steric and electrostatic interactions.[16] The latter have proven useful in anticipating which brush architectures will resist fouling.[4] With the advent of well-characterized brushes, protein adsorption studies focused on the fundamental brush parameters of tether length and spacing, corroborating physical models of brush-protein interactions.[5-7,12,13,17-22] At the same time, however, careful studies with well-characterized brushes supported a rule of thumb that about 1mg/m^2 of end-grafted PEG is sufficient to eliminate bioadhesion *in-vitro*.[18-20,23] This observation was independent of tether length and spacing over a relatively broad range. It has been vexing, however, that protein-resistant PEG brushes (based on in-vitro characterization) still support non-specific bio-adhesion in applied and animal studies.[2,24]

Perfectly designed brushes can be difficult to implement: Even with the proper tether chemistry for the application, appropriate anchoring, and judicious choice of chain length and tether spacing, impurities can locally block brush deposition (or growth), creating flaws and heterogeneities as small as tens of nanometers.[9] While such tiny isolated bare patches on the substrate tend to be obstructed by the lateral expansion of the tethers, they are still locally less repulsive (and even attractive) to objects in solution compared with the “perfect” brush. Our lab has developed a controlled method to distribute such isolated flaws randomly on a brushy surface, and we have demonstrated that these “synthetic flaws” are useful in understanding the engineering challenges of brush fabrication.[25] We have additionally demonstrated the utility of flaws, as a motif for the design of functional brushes.[26] Embedding discrete functionality at the base of a brush rather than placing it on extended tethers sets up competition between local attractions and the steric forces of the brush which leads to highly selective capture on the molecular level, for instance for proteins from solution.[26]

The flawed or “patchy” brushes, depicted schematically in Figure 1, are based on a convenient PEG anchoring scheme originally developed in the Hubbell and Textor labs.[27,28] With poly-l-lysine (PLL)-PEG graft copolymers adsorbing on silica primarily by their main cationic backbones, the PEG tethers extend into solution to form the brush. Our contribution is the random placement of isolated PLL coils on the silica prior to adsorption of the PLL-PEG. We demonstrated that the PLL (which is more strongly adsorbing than the PLL-PEG) is retained during PLL-PEG backfill and that both the PLL and PLL-PEG are retained on the surface over and beyond the conditions (protein bacterial exposure and ionic strength variations) in the current study.[29] In the current study, isolated PLL coils at the base of the brush not only provide nano-scale tether-free imperfections, they localize dense cationic functionality that is electrostatically attractive to negative proteins and bacteria, including *S. aureus*. These PLL coils carry greater positive charge than the PLL backbone of the PLL-PEG copolymer, since PEG grafting (on the PLL backbone of the copolymer) occurs at the sites of amines.

It is extremely important to note that the brushes we employ, before the incorporation of PLL patches, completely resist protein and *S. aureus* adhesion (to within 0.01 mg/m^2)[29] and were among the most protein- and bacteria-repellant architectures in the large library of “bottle brush” copolymers developed by Textor and Hubbell.[27,28] While it was observed and later explained with self consistent field models,[30] that some molecular architectures (especially those with large PEG functionalization of the PLL backbone) produced adsorbed

layers which failed to form classical brushes or to repel proteins, our study starts with brushes that avoid primary,[6] secondary,[6] and tertiary[31] protein adhesion and introduces discrete, well-characterized electrostatically adhesive "flaws" in a controlled fashion. Further, our choices of molecular architectures range from 25-50% in PEG functionalization, and have been shown to behave similarly, in their protein resistance, to single PEG chains anchored individually at appropriate densities,[20] as is the case for a classical polymer brush. We have not detected any suggestion that the specific PLL-PEG graft copolymer architectures we have chosen produce lateral heterogeneities in the brush and that instead, the interesting features of the brush adhesiveness in our studies arise from the homopolymer PLL patches we intentionally place on the substrate. This further substantiates the use of classical brush models, here, to develop our thinking about these interfaces.

While our previous papers have focused on the impact of the polymer brush architecture on protein adsorption,[25,26,29,32] this paper focuses on *Staphylococcus aureus* capture at the same interfaces and reveals information about the brush compression during initial bacterial capture that compliments the classical literature on PEG brush compression.[9,12,13,33] Our emphasis on initial capture focuses on physico-chemical interactions and avoids longer-time processes such as viscoelastic relaxation of the bacteria's shape or "living" responses of the bacteria. (The choice of *S. aureus* bacteria allows focus on the simplest spherical shape. The study does not address complexities associated with bacterial protrusions.)

This work also highlights important distinctions in how steric forces potentially play out for micron-scale and molecular-scale objects. In this study, the flaws or PLL "patches" are used as a measure of the brush compression energy during bacterial capture: The brushes themselves (without flaws) are robust against bacteria (and protein capture). The adhesive patches at the base of the brush, when present in sufficient numbers, pull *S. Aureus* bacteria (negatively charged 1 um spheres in the initial instants of their capture) to the interface, and are opposed by the steric repulsions from the brush on the remaining contact area. Thus the number of patches needed for bacterial capture provides a measure of the relative energy of brush compression, reported in this paper for three brushes which vary in height and PEG content. Additionally in this work, the *S. aureus* adhesion is compared with previous studies of protein capture on the same surfaces,[26,32] to reveal potential differences between-micron-scale and molecular-scale steric interactions on these brushes. The latter provide insights into the failure of *in vitro* studies with serum proteins to predict the fouling of materials in implant studies.

Experimental Materials and Methods

Poly-l-lysine hydrobromide (PLL) samples with molecular weights of 20,000 and 50,000 were purchased from Sigma and used as the adhesive cationic patches in these studies. Additionally, the 20,000 molecular weight PLL served as the anchoring component of the three copolymer brushes in this study.

Three graft copolymers, synthesized and purified as previously described[25] and summarized in Table I, were used to create the brushes in this study. They were all based on 20,000 molecular weight PLL but vary the length and density of their PEG side chains. These particular copolymers were chosen because the brushes they form upon adsorption to negative surfaces almost completely eliminate adhesion of serum proteins[27,28] and bacteria.[34] In Table I, the "grafting ratio" is the number of PLL units per PEG side chain. This quantity is the inverse of the fraction of PLL units functionalized, but is reported here for consistency with prior convention.[27,28] The grafting ratio of the copolymers dissolved in D_2O was determined using ^1H NMR on a Bruker 400 mHz instrument, based on the relative

areas of the lysine side-chain peak (-CH_2-N-) at 2.909 ppm and the PEG peak (-CH_2-CH_2-) at 3.615 ppm.

The surfaces of interest were formed by sequential adsorption of PLL and PLL-PEG from flowing pH 7.4 phosphate buffered solutions (phosphate buffer is 0.008M Na_2HPO_4 and 0.002M KH_2PO_4 having Debye length κ^{-1} = 2 nm) on acid etched microscope slides, also described previously.[25,32] These substrates, Fisher Finest, were soaked overnight in concentrated sulfuric acid and rinsed with DI water to remove the metal ions from the near-surface region, leaving a nearly pure silica surface. The slides were then placed in a slit shear flow chamber and buffer introduced into the fluid space. Flowing buffer, at a gentle wall shear rate of 5 s^{-1}, was followed by 5 ppm PLL solution for a targeted amount of time to limit the adsorption of PLL chains below that of a saturated PLL layer. Buffer was then reintroduced, followed by a 100 ppm solution of the PLL-PEG of interest to backfill the remaining silica surface with a PEG brush. The amount of time necessary to deposit the desired amount of PLL was originally determined by monitoring the adsorption process using near-Brewster reflectometry.[25] In most of the current studies, especially those of bacterial capture, the surface fabrication was run “blind” based on previous calibrations for adsorption times. Studies of fibrinogen adsorption (Sigma, F8630-1G, used as supplied) employed near-Brewster reflectometry,[35] and here it was possible to monitor the polymer deposition to create each surface just before the protein adsorption studies in the same flow chamber. In the fibrinogen adsorption studies, 100 ppm protein solution in pH 7.4 phosphate buffer was flowed over the surface of interest for 20-30 minutes and the reflectivity signal monitored. Buffer was subsequently reintroduced.

Table II summarizes the properties of the three brushes without adhesive patches. These parameters which describe the brush structures, were calculated from measurements of the adsorbed PLL-PEG mass and knowledge of the PEG content in each copolymer, from Table I. Parameters, such as the average spacing between grafting sites, follow (as described in the Supporting Information) without any assumptions for a particular model of the brush. Other properties, such as the number of “blobs” in the brush, its height, and its energy are model-specific. Here, the “Flory” brush from Alexander and DeGennes and the semidilute brush model of DeGennes are compared and found to be in good agreement.[36,37] The height calculations based on the Alexander-DeGennes treatment detailed in the Supporting Information carry second and third virial coefficients measured by osmometry (Advanced Instruments) for PEO solutions (8000 molecular weight, Polysciences) up to 17 wt%. These values were found to adequately predict measured depletion forces in a separate work.[38] Notable in Table II is that Brushes 1 and 2 are similar in PEG content while Brushes 2 and 3 are similar in height, allowing the importance of these parameters to be tested.

S. aureus (ATCC 25923) was chosen for this study because of its spherical shape and negative charge. The particular strain was originally a clinical isolate, and has become widely used in standardized tests of bacterial antibiotic susceptibility. This particular strain was additionally chosen for its nonpathogenic behavior, while still closely resembling strains found in hospital infections. Bacteria were grown according to standard procedure in Luria-Bertani (LB) medium. Cultures were incubated aerobically overnight at 37 °C, shaking at 200 rpm. Bacteria were harvested after a total of 24h during logarithmic growth. Bacteria were subsequently centrifuged at 100 × g and re-suspended in phosphate buffer twice. This rinsing procedure was shown to remove protein and other molecules which might potentially contaminate the surfaces. All bacteria were studied within 24h of preparation and stored in a refrigerator near 4°C. The nominal target bacterial concentration was 5×10^5/ ml during the runs.

In studies of bacterial adhesion, bacteria suspensions were flowed over test surfaces in a custom-built “lateral” microscope. This instrument orients test surfaces perpendicular to the floor so that no gravitational forces contribute to or detract from bacteria-surface interactions. Bacteria capture was monitored on video and, using ImageJ software, the numbers of bacteria in each frame were determined, enabling the bacterial capture kinetics to be plotted. Bacterial accumulation was typically linear in time for at least 10 minutes, allowing the initial bacterial capture rates to be determined. These initial capture rates, which do not reflect bacteria-bacteria interactions at the surface, provide information about the interactions of individual bacteria with the substrates. Procedures follow those of prior studies in our lab for other surfaces.[39-41]

This paper reports bacterial capture efficiencies. The capture efficiency is the initial bacterial capture rate on a test surface, normalized by the transport-limited (maximum possible) capture rate for the same suspension. The latter is measured on a surface that is strongly and rapidly adhesive towards bacteria. This analysis method is necessary because different batches of bacteria measured on different days contain slightly different bacterial concentrations, which are difficult to quantify with the necessary precision.[39] Measuring the transport-limited bacterial capture rates for each batch of bacteria suspension and presenting data in the form of bacterial capture efficiencies facilitate quantitative comparisons of different bacterial batches on different test surfaces. A saturated adsorbed PLL layer, which is densely positively charged, was employed as the strongly attractive surface. Transport limited bacterial capture on this type of surface, for the range of adsorption conditions studied here has been previously established.[25]

Results

For two different patch molecular weights, 20,000 and 50,000 in Brush 2, Figure 2A summarizes the adhesion or capture efficiencies of *S. aureus* from flowing phosphate buffer. Because brushes completely resist bacterial adhesion, in Figure 2A patches must be present within the brushes to produce bacterial capture. The onset of bacterial capture occurs at patch surface loadings or “thresholds” rather than the data passing through the origin.

Adhesion thresholds are indicators of multivalent bacterial capture,[42] that is, the involvement of several patches in the capture of each bacterial cell. This interpretation becomes clear when one considers that the surfaces containing fewer than the threshold density of adhesive patches are incapable of adhering bacteria. Thus, while single patches may attract bacteria, individual attractions are too weak to capture and hold single bacterial cells, even in gentle flow.

The shifting of the thresholds to smaller patch loadings (to the left) for larger 50K patches in Figure 2A is consistent with the expectation that higher molecular weight patches will have stronger attractions towards bacteria. With fewer large patches needed for bacterial capture (compared with a greater number of small patches) the threshold for large patches lies to the left of that for the small patches. In the limit of very strong patch-bacteria interactions, bacteria can be captured and held by surface species, and data extrapolate to the origin rather than a finite x-intercept.[39]

It is interesting to consider the extent to which the mass of cationic patches (or the total cationic functionality of the interface) dictates the capture efficiency. This is explored in Figure 2B for the same data from Figure 2A. While the mass-based representation in Figure 2B brings the data sets closer, they do not completely collapse. There remain different patch-dependent thresholds for the two patch sizes, and the data appear to cross, within experimental error. The persistent spread of bacterial capture data, in Figure 2B, parallels

that seen for the capture of 1-um silica spheres on silica surfaces containing cationic acrylic patches (poly[dimethylamino ethyl metharcrylate]) of different molecular weights.[43] While the capture of silica spheres on the different patches sizes was quite distinct when plotted as a function of patch number (similar to Figure 2A), plotting silica particle capture rates as a function of patch mass brought the data together and caused them to cross (similar to Figure 2B). This behavior was shown to be a result of the random patch statistics, and of the requirement for an appropriate cationic density in the particle -surface interaction region.[42] Our observed crossing of the data in Figure 2B is consistent with the random arrangement and relative adhesion strengths of the patches, as expected.

The results in Figure 2 are further significant in that they uphold that the binding energy of each patch is roughly proportional to the PLL molecular weight. This further confirms that the electrostatic nature of the bacteria-patch attraction. The result in Figure 2 therefore argues against any significant contributions of tertiary (or “ternary”) attractions between the PEG brush itself and the bacteria,[31] potentially occurring because of the different brush density in the vicinity of a patch.[44]

Figure 3 explores the impact of the brush architecture on bacterial capture for PLL patches of 20,000 molecular weight. Part B of Figure 3, previously published,[32] facilitates a direct comparison to fibrinogen adsorption for the same series of surfaces, in the discussion below. In Figure 3, the threshold concentrations of adhesive patches for bacterial capture increases with brush height, since the range of steric repulsions increases accordingly.

A comparison of parts A and B of Figure 3 reveals several interesting observations. First, thresholds for fibrinogen capture occur at much higher patch concentrations than the thresholds for bacteria. The observation of fibrinogen thresholds suggests weak patch-protein interactions: Fibrinogen adheres by bridging two or more adhesive surface sites.[32] This interpretation is consistent with the average patch spacing at the fibrinogen thresholds (12-22 nm), which is less than fibrinogen’s 45 nm length. Since proteins are relatively small, then, the surface loading of these randomly-arranged patches must be relatively large to ensure statistically significant numbers of protein-sized surface regions in which multiple adhesive sites are closely situated. Since the bacterial cells are larger than proteins, multivalent bacterial capture can potentially occur at lower patch loadings, consistent with the scale of the second x-axis (average patch spacing) in Figure 3. The actual bacterial thresholds will depend on the particular numbers of patches needed for capture and the bacterial-surface contact area, discussed below.

A second important observation in Figure 3 is that the sensitivity of the threshold position to the brush architecture is greater for the proteins than it is for *S. aureus*. That is, we observe a greater shifting in the protein thresholds in part B for Brushes 1-3 compared with the spread of the data in Figure 3A. This observation has the technologically-useful benefit that brushes could be chosen to tune the relative adhesion of proteins and cells on these surfaces.

Analysis and Discussion

While it has long been known that the brushy biocompatible surfaces which avoid protein adhesion are also useful in repelling cells such as bacteria,[2] the remarkable size range (3 orders of magnitude from molecular to cellular-scale) of the objects that can be manipulated by steric forces has historically been taken for granted. Figures 2 and 3 reveal important similarities and differences in how brushy steric repulsions come into play for bacteria versus proteins experiencing localized attractions. If one views the adhesive “patches” as synthetic receptors or, at least, technologically-useful constructs for manipulation of biological entities, it is remarkable that the same brushy interfaces with the same adhesive

"elements" produce parallel behaviors at the molecular and cellular level. On the other hand, if one views the cationic patches as (quantifiable models for) flaws in an otherwise bio-resistant brush, we have the striking observation that such small flaws (individually too adhesively weak to immobilize much of anything), are far more catastrophic in that they more readily facilitate unwanted cell adhesion compared to protein adhesion. (Of the several proteins we have studied on these brushes,[26,29] fibrinogen is the largest [4.5 nm x 4.5 nm x 47 nm] and correspondingly most adhesive, with other proteins such as albumin adhering only at even higher patch loadings.[26]) For most surfaces, even engineered surfaces, protein adsorption is typically thought to be a precursor for cellular adhesion.[1,2] On the "flawed" brushes in this study, cells adhere directly without prerequisite protein adsorption. We are aware of one other study documenting a similar trend on PEG-coated steel.[24]

The role of Adhesive "Flaws": Valency numbers for Bacterial versus Protein Capture

A basic quantity at the core of understanding *S. aureus* versus protein capture is the numbers of adhesive patches (the "valency") required for their capture. Even without understanding the physics of the brushes or the patch-bacteria interaction, it is possible to estimate the valency. We have developed a statistical treatment that was published previously[42] and is reviewed here in the Supporting Information. The model assumes only (1) a random arrangement of adhesive sites on the surface, described by a Poisson distribution (a material feature which has been previously established[25]) and (2) a known area between the surface and the target over which the attractive forces act. *S. aureus* is approximated as a simple sphere, a simplification which provides an estimate of the contact area, but which might more seriously break down for other bacterial strains with protrusions such as pili that might penetrate the brush rather than compress it. The treatment predicts the normalized capture probability as a function of the overall loading of patches. The latter is the quantity on the x-axis of Figures 2 and 3. The capture probability is roughly proportional to the capture rate or efficiency on the y-axis of these figures.[42] A prior work, which accessed a regime of monovalent bacterial capture on more strongly adhesive elements, presented a scheme to translate capture probability to efficiency.[40] This conversion translates to other systems with weaker adhesive elements such as the current study. In presenting the predictions of the statistical model, we include both scales on the y-axes.

Figure 4A provides perspective on the area over which *S. aureus*-surface attractions act. When a bacterium, approximated as a sphere of radius R_p = 500 nm, first touches the surface, the area over which attractive (electrostatic) forces act is defined by the overlap of the electrostatic double layers of the sphere and the collector. The radius of this electrostatic force zone follows from geometry, $\left(r_f^{es}\right)^2+\left(R_p-\kappa^{-1}\right)^2=\left(R_p+\kappa^{-1}\right)^2$ or $r_f^{es}=2\left(R_p\kappa^{-1}\right)^{1/2}$. Here the Debye length, κ^{-1}, is 2 nm. For a 1-micron spherical bacterium r_f^{es}=63.25nm and the electrostatic area, $\left(r_f^{es}\right)^2$, is 4000 nm^2.

Figure 5 presents calculated bacterial capture efficiencies as a function of the loading of cationic patches on the collector. Figure 5A, to be compared with the data of Figure 3A, employs $\left(r_f^{es}\right)^2$=4000 nm^2. The different curves represent variations in valency, the numbers of patches required for bacterial capture. It is seen that as greater numbers of patches are required, the curves and adhesion thresholds shift to higher overall patch loadings. Comparing Figure 5A to Brush 1 in Figure 3A suggests that about 10-15 20,000 molecular weight patches required for bacterial capture. For Brushes 2 and 3, the minimum number of patches could be as high as 20. Likewise a comparison between Figure 5A and Figure 2A suggests that in Brush #2, the minimum necessary number of patches decreases from ~13 to ~5 as the patch molecular weight is increased from 20,000 to 50,000. This change in valency

is roughly inversely proportional to the patch molecular weight, since the binding enthalpy scales as the patch molecular weight.[43]

Figure 5B explores the sensitivity of these calculations to the estimated bacteria-surface attraction area. The contact areas of 20,000 nm^2 and 1000 nm^2 represent extreme possibilities. Figure 5B reveals that the small area of 1000 nm^2 is unrealistic: The slopes and thresholds in the calculated capture plots substantially miss the observations for in Figure 3A. Second, larger attraction areas of 20,000 could explain the data (thought we feel that the 4000 nm^2 electrostatic contact area in Figure 5A is a better estimate given our current understanding of the interface.) If the contact area were 20,000 nm^2, then 35-50 patches would be needed for bacterial capture on Brush 1 with 20,000 MW PLL patches.

While the statistical approach has some limitations due to uncertainty in bacteria-surface attraction area, estimates of the bacterial capture valency are relatively robust: A valency between 10 and 50 for 20,000 MW PLL patches broadly encompasses our full range of expectations for Brush 1, with greater confidence at the low end near 10-20. This valency makes sense in light of receptor-ligand bond numbers reported for other biological systems, such as white blood cell interactions.[45-47] This valency range for bacteria capture also provides an interesting contrast to our reports for fibrinogen capture in Figure 3B.[32] We previously reported 2-3 protein-surface contacts necessary for fibrinogen capture on the same surfaces, for initial protein-surface contact areas in the range 150-200 nm^2. The current analysis shows that bacterial capture involves at least an order of magnitude greater numbers of adhesive elements but, because of the large bacteria-surface contact areas compared to proteins, the adhesion thresholds for bacterial capture are much smaller than those for proteins.

The Impact of Brush Architecture on Steric Repulsions of Bacteria

The multiple attractions from the adhesive patches offset the different amounts of steric repulsion between the different brushes and a bacterium (or protein). In understanding this repulsion, two aspects must be considered: (1) the area over which the repulsion acts and (2) the physics of the repulsion: compression or penetration.

During bacterial capture, different steric interaction areas (of radius r_s) for the different brushes result from the brush-dependence of the range of steric forces. In a first approximation illustrated in Figure 4B, a spherical bacterium of radius R_p = 500 nm compresses the brush, of initial height h to final separation h', so that the bacterial surface comes within about a Debye length ($h'=\kappa^{-1}$=2 nm) of the charged patches. The brush deformation, δ, follows as h – 2 nm. Then from geometrical arguments motivated by Figure 4B, $r_s^2 + (R_p - \delta)^2 = R_p^2$, so that $r_s = (\delta^2 + 2\delta R_p)^{1/2}$. For instance for Brush 1 with δ = 7 nm, one obtains an approximate interaction radius, $r_s \sim 84$ nm, and a total steric interaction area of about 7000 nm^2. Larger steric areas result for Brushes 2 and 3, still with h'= 2 nm, summarized in Table III. To a first approximation, the total steric repulsion should scale as the steric contact area. Proportionate numbers of adhesive elements, as calculated in the previous section, are expected to be needed within the electrostatic contact area to produce bacterial capture. Notably, the definitions of steric and electrostatic areas differ fundamentally. The steric area varies with differences in the brush, but the electrostatic interaction area depends on Debye length.

We estimate, as a first approximation, that bacteria-brush interactions resemble brush compression by an impenetrable wall, neglecting complexities of the bacterial surface which are insufficiently known to develop a more sophisticated picture. We proceed with this approach, as the use of brush compression models for cell interactions has shown recent success for the adhesion and release of mammalian cells which may be softer than

bacteria.[48] The work brush of compression depends on the brush architecture, primarily through the parameters N and σ, the statistical number of segments per tether and areal density of tethers, respectively. These are summarized in Table II.

Worth noting is that h and σ, along with the total tethered PEG, are preserved at the bacterial adhesion thresholds. That is, for a series of surfaces with increasing numbers of cationic patches at the base of a brush, the amount of brush needed to backfill the remaining surface decreases once the patch loading reaches a critical level, on the order of 800 mg/m^2 for Brush 1, 1200 mg/m^2 for Brush 2, and 2200 mg/m^2 for Brush 3.[32] This decrease in backfill tends to compromise the brush, especially near the high protein adsorption thresholds in Figure 3B. However, the threshold patch densities for bacterial capture in Figures 2 and 3A occur at relatively low patch loadings and therefore correspond to negligible decreases in the PLL-PEG backfill relative to a brush containing no patches. The properties of the various brushes at the adhesion thresholds for bacteria and fibrinogen are summarized in Table III, and for the bacterial adhesion are similar to the properties in Table II.

With the properties of the brush determined at conditions where bacteria start to adhere, in Table III, it becomes possible to estimate the steric cost of compression. We considered two approaches for this calculation, both based on the Alexander DeGennes treatment of a Flory brush.[36,37] The Alexander-deGennes treatment, which neglects the real concentration profile in the brush in favor of a constant segmental concentration, is unrealistic. However, for uncompressed brushes, both osmotic and stretching energies are over estimated and errors cancel, so that estimates of brush height are often reasonable.[17] Additionally, for the large compressions in our work (starting with brushes on the order of 10 nm and compressing down to a thickness on the order of a Debye length), the structural features of the brush, for instance the tether spacing and segmental concentration profile, become relatively unimportant. Milner has demonstrated, for instance, that the step function and parabolic brush forms give similar results for large compressions such as those in the current study.[17] The essential feature is that the compression is resisted by the osmotic pressure in the gap.

Our simplest calculation of the brush compression cost follows the form in which the free energy of the brush (and its height) are controlled by segment-segment interactions via a second virial coefficient. We commence with this route because it suggests a scaling behavior that is obscured when more accurate solution thermodynamics are included. This approach, including the Derjaguin approximation for the sphere-plate geometry (approximating the bacteria-substrate approach), detailed in the Supporting Information, yields the result that the cost of compressing a brush (2 or 3), $E^{\text{sph-plt}}{}_{\text{stericBRUSH2}}$ relative to the compression cost of brush 1, $E^{\text{sph-plt}}{}_{\text{stericBRUSH1}}$, is:

$$\frac{E^{spn-plt}_{\text{steric-BRUSH}_2}}{E^{spn-plt}_{\text{steric-BRUSH}_1}} = \frac{r^2_{BR_2}}{r^2_{BR_1}} \, ln \frac{u'_{min-BR_1}}{u'_{min-BR_2}} \quad (1)$$

Note here that the compression cost depends only on the amount of PEO (Γ, mg/m^2) tethered at the interface (the independent dependencies on N and σ drop out, as does the second virial coefficient itself) along with the compression ratio itself. Here u'_{min} for a particular brush is the brush height beneath the center of the sphere relative to the uncompressed height. For similar compression ratios of the two brushes, the logarithmic term becomes close to unity. Table III therefore estimates the cost of brush compression, relative to brush 1, accordingly.

While equation 1 makes the assumption of that the osmotic pressure is well-described by a second virial coefficient, strongly compressed gaps (to near a Debye length) sustain higher

PEO concentrations. In a second, more precise calculation, we therefore employed the full Flory expression for the osmotic pressure,

$$\frac{\pi}{RT} = -\frac{1}{V_s^L}\left[\ln\left(1-\varphi_p\right)+\left(1-\frac{1}{N}\right)\varphi_p+\chi\varphi_p^2\right] \quad (2)$$

Integrating via the Derjaguin approximation yields a long expression, in the Supporting Information, for the cost of brush compression. Substituting the initial brush heights and a final brush height of 2 nm into this expression (along with chi = 0.4[49]), we report the values in Table III for the relative cost of brush compression. Notably, the previous scaling as the square of PEO brush content is obscured by the improved solution thermodynamics; however, the relative compression costs are similar to the simpler second virial approach.

Assuming that the critical number of adhesive patches needed for capture is proportional to the steric repulsion, the ranking of the bacterial thresholds should follow similarly. This is the case qualitatively: In Figure 3A, though the ratios of the valencies for Brushes 2 and 3 relative to Brush 1 (18:13 and 20:13, respectively) are not exactly 1 and 3, respectively. One can explain this modest discrepancy, however, by relaxing the assumption that bacterial capture on the three brushes results in the exactly the same gap thickness (closest bacteria-surface contact) for all three brushes. The approximate agreement between these brush thresholds and the relative valencies for the bacterial capture supports the assumption of strong compression, providing insight into the nature and extent of bacterial-surface interactions.

Steric Interactions with Proteins

The large protein thresholds and sensitivity of protein capture to brush architecture suggest differences, relative to bacteria, in the steric interactions between brushes and fibrinogen. First, multivalent fibrinogen adsorption suggests a side-on protein orientation to the surface allowing the long fibrinogen molecule to bridge several patches. Protein approach to within a Debye length of the underlying substrate requires entry of the protein into the brush by compression or penetration. Thus the full side-on area, between 150 and 200 nm for fibrinogen independent of brush architecture, comprises the area governing the steric interactions in Figure 6. This is much smaller than the bacterial contact areas in Figure 4.

If fibrinogen penetrates a Flory brush in a side-on orientation, the entropic cost is the osmotic penalty associated with the protein excluded volume.[6,50] Estimating the excluded fibrinogen volume as $4.5 \times 4.5 \times 45 = 900\ nm^3$, and using second and third virial coefficients of 0.0057 $cm^3\ mol/g^2$ and 0.059 $cm^6\ mol\ /g^3$, respectively, to estimate the osmotic pressure,[38] (also used to calculate the brush height), the results are summarized in Table III.

The calculations raise two points: First, the calculated insertion costs suggest a ranking of the fibrinogen thresholds as Brush 1, Brush 3 and then Brush 2. While we do not observe this for κ^{-1}=2 nm, we did report this trend at higher ionic strength,[32] suggesting more extensive protein penetration at the smaller Debye length of κ^{-1} =1 nm into the same series of brushes. Second, the calculated steric insertion costs in Table III seem large: They represent an upper limit because the tether spacing in the calculation is an average value for the brush, not accounting for the greater tether spacing (order 10 nm) in the vicinity of the patches where the fibrinogen is actually located. Additionally, in the case of the thinner brush 1 at the fibrinogen threshold (around 6 nm), it may be that fibrinogen (4.5 nm high) need not insert fully, suggesting the insertion penalty could be reduced on the order of 50%. The dependence of the insertion cost on brush structure (with persistence lengths between 2

and 10 nm) could produce extreme sensitivity of fibrinogen interactions to local brush structure.

With side-on fibrinogen adsorption bridging multiple patches, the cost of brush compression is also worth estimating. First, the side-on contact area, $4.5 \times 45 \sim 200$ nm^2, is estimated to be brush-independent, due to small fibrinogen dimensions perpendicular to the brush. Compressing this area of brush in a piston-like fashion (rather than applying Derjaguin, since fibrinogen is not a sphere), gives the results summarized in Table III. Note that in obtaining these figures, the osmotic pressure is the resistance to compression, as described by Milner.[17] Rather than employing the second virial expression for osmotic pressure, we use equation 2, with $\chi = 0.4$[49] because of the elevated segmental concentrations in a gap whose thickness is the 2 nm Debye length. While the results appear slightly less costly than penetration, the sufficient uncertainty (the actual position of the protein within the brush, and the details of its surface contour) in the calculations precludes a firm argument for penetration or compression by protein. Penetration may be favorable only because it can exploit structural details of the brush in the vicinity of the patches to further lower the energetic cost. Compression would tend to be sensitive average the local chain concentration in the vicinity of the patch and protein and therefore potentially sustain a higher steric penalty.

Conclusions and Significance

In the study of *S. aureus* interactions with flawed or patchy protein-resistant brushy surfaces, this work considered both the size (or binding energy) of the patches and the architecture of the brush. By varying the patch molecular weight, the numbers of cationic charges in localized surface regions were varied. Larger patches produced bacterial adhesion at lower patch loadings, and analysis confirmed the importance of both the patch size (numbers of charges) and the random patch arrangement. This reinforced the discrete, rather than mean field, nature of the bacteria-surface attractions.

The “valencies” (the minimum numbers of patches engaging each bacterium during capture), determined from a comparison of calculations to experiments, provided an estimate of the relative brush compression penalty, ie the steric forces between *S. aureus* and surfaces containing different engineered brushes. Results were consistent with dramatic brush compression to heights on the order of the 2 nm Debye length. A treatment using the full Flory expression to estimate the osmotic pressure of a substantially compressed brush agreed reasonably with the estimates based on valency calculations. A simplified second virial expression for the osmotic pressure on compression was not inconsistent with the data. Both approaches, which were dominated by an osmotic term, reinforced a simple design rule for brushes, focusing on the amount of PEO tethered at the interface (assuming sufficient brush height and small persistence length relative to the protein size.) This further emphasized the relative unimportance detailed brush structure (segmental concentration profile, tether density as long as it is smaller than the protein size). The consistency with large brush compressions explains observations in the literature concerning the important of overall brush mass.

Protein adhesion on the same series of brushes was found to require greater patch densities than those needed for bacterial capture. This observation carries scientific and practical weight. The greater patch density required for protein capture was a result of the localization of attractive interactions into patchy regions. With weakly attractive surface patches, a higher overall patch density is needed for protein capture because proteins must be able to bridge multiple patches in order to adsorb. Such bridging by larger bacteria can occur with smaller overall patchy loadings. Also observed, the threshold or patch loading for the onset

of adsorption was much more sensitive, for proteins, to brush architecture than the thresholds for bacterial capture. This is thought to be a result of a protein's ability to penetrate the brush in a manner dependent on local brush structure. By contrast, bacterial adhesion requires a more uniform brush compression.

These observations imply that for brush-based protein resistant biomaterials, nanoscale flaws can induce bacterial fouling and cell adhesion long before protein adsorption occurs. This behavior differs markedly from classical understanding that protein adsorption precedes cell adhesion and explains why protein adsorption can sometimes be a poor predictor of cell-surface interactions.

Supplementary Material

Refer to Web version on PubMed Central for supplementary material.

Acknowledgments

This work was supported by NSF-08-05061, and NIH R21 CA159109-01A1 and the UMass MRSEC on Polymers.

References

1. Kingshott P, Griesser HJ. Curr. Opin. Solid State Mat. Sci. 1999; 4:403.
2. Ratner BD, Bryant SJ. Annu. Rev. Biomed. Eng. 2004; 6:41. [PubMed: 15255762]
3. Ostuni E, Chapman RG, Holmlin RE, Takayama S, Whitesides GM. Langmuir. 2001; 17:5605.
4. Pasche S, Textor M, Meagher L, Spencer ND, Griesser HJ. Langmuir. 2005; 21:6508. [PubMed: 15982060]
5. Currie EPK, Norde W, Stuart MAC. Adv. Colloid Interface Sci. 2003; 100:205. [PubMed: 12668330]
6. Halperin A. Langmuir. 1999; 15:2525.
7. Malmsten M, Emoto K, Van Alstine JM. J. Colloid Interface Sci. 1998; 202:507.
8. Efremova NV, Bondurant B, O'Brien DF, Leckband DE. Biochemistry. 2000; 39:3441. [PubMed: 10727239]
9. Kelley TW, Schorr PA, Johnson KD, Tirrell M, Frisbie CD. Macromolecules. 1998; 31:4297.
10. Ruths M, Johannsmann D, Ruhe J, Knoll W. Macromolecules. 2000; 33:3860.
11. Martin JI, Wang ZG. J. Phys. Chem. 1995; 99:2833.
12. Yamamoto S, Ejaz M, Tsujii Y, Fukuda T. Macromolecules. 2000; 33:5608.
13. Yamamoto S, Ejaz M, Tsujii Y, Matsumoto M, Fukuda T. Macromolecules. 2000; 33:5602.
14. Drobek T, Spencer ND, Heuberger M. Macromolecules. 2005; 38:5254.
15. Heuberger M, Drobek T, Spencer ND. Biophys. J. 2005; 88:495. [PubMed: 15501935]
16. Pasche S, Voros J, Griesser HJ, Spencer ND, Textor MJ. Phys. Chem. B. 2005; 109:17545.
17. Milner ST. Science. 1991; 251:905. [PubMed: 17847384]
18. Kingshott P, Thissen H, Griesser HJ. Biomaterials. 2002; 23:2043. [PubMed: 11996046]
19. McPherson T, Kidane A, Szleifer I, Park K. Langmuir. 1998; 14:176.
20. Dalsin JL, Lin LJ, Tosatti S, Voros J, Textor M, Messersmith PB. Langmuir. 2005; 21:640. [PubMed: 15641834]
21. Sofia SJ, Premnath V, Merrill EW. Macromolecules. 1998; 31:5059. [PubMed: 9680446]
22. Wagner VE, Koberstein JT, Bryers JD. Biomaterials. 2004; 25:2247. [PubMed: 14741590]
23. Malmsten M, VanAlstine JM. J. Colloid Interface Sci. 1996; 177:502.
24. Wei J, Ravn DB, Gram L, Kingshott P. Colloid Surf. B-Biointerfaces. 2003; 32:275.
25. Gon S, Bendersky M, Ross JL, Santore MM. Langmuir. 2010; 26:12147. [PubMed: 20557060]
26. Gon S, Santore MM. Langmuir. 2011; 27:1487. [PubMed: 21207949]

27. Huang NP, Michel R, Voros J, Textor M, Hofer R, Rossi A, Elbert DL, Hubbell JA, Spencer ND. Langmuir. 2001; 17:489.
28. Kenausis GL, Voros J, Elbert DL, Huang NP, Hofer R, Ruiz-Taylor L, Textor M, Hubbell JA, Spencer ND. J. Phys. Chem. B. 2000; 104:3298.
29. Gon S, Fang B, Santore MM. Macromolecules. 2011; 44:8161.
30. Feuz L, Leermakers FAM, Textor M, Borisov O. Langmuir. 2008; 24:7232. [PubMed: 18558731]
31. Halperin A, Kroger M. Langmuir. 2009; 25:11621. [PubMed: 19673469]
32. Gon S, Santore MM. Langmuir. 2011; 27:15083. [PubMed: 22040182]
33. Watanabe H, Tirrell M. Macromolecules. 1993; 26:6455.
34. Harris LG, Tosatti S, Wieland M, Textor M, Richards RG. Biomaterials. 2004; 25:4135. [PubMed: 15046904]
35. Fu ZG, Santore MM. Colloid Surf. A-Physicochem. Eng. Asp. 1998; 135:63.
36. Alexander S. Journal De Physique. 1977; 38:983.
37. de Gennes PG. J. Phys. (Paris). 1976; 38:1443.
38. Nam J, Santore MM. Phys. Rev. Lett. 2011; 107
39. Fang B, Gon S, Park M, Kumar KN, Rotello VM, Nusslein K, Santore MM. Colloid Surf. B-Biointerfaces. 2011; 87:109.
40. Fang B, Gon S, Park MH, Kumar KN, Rotello VM, Nusslein K, Santore MM. Langmuir. 2012; 28:7803. [PubMed: 22563906]
41. Kalasin S, Dabkowski J, Nusslein K, Santore MM. Colloid Surf. B-Biointerfaces. 2010; 76:489.
42. Duffadar R, Kalasin S, Davis JM, Santore MM. J. Colloid Interface Sci. 2009; 337:396. [PubMed: 19539949]
43. Kalasin S, Martwiset S, Coughlin EB, Santore MM. Langmuir. 2010; 26:16865. [PubMed: 20961162]
44. Bosker WTE, Iakovlev PA, Norde W, Stuart MAC. J. Colloid Interface Sci. 2005; 286:496. [PubMed: 15897063]
45. King MR, Rodgers SD, Hammer DA. Langmuir. 2001; 17:4139.
46. Hammer DA, Tirrell M. Annu. Rev. Mater. Sci. 1996; 26:651.
47. King MR, Hammer DA. Biophys. J. 2001; 81:799. [PubMed: 11463626]
48. Halperin A, Kroger M. Biomaterials. 2012; 33:4975. [PubMed: 22502791]
49. Pedersen JS, Sommer C. Progr. Colloid Polymer Sci. 2005; 130:70.
50. Halperin A, Fragneto G, Schollier A, Sferrazza M. Langmuir. 2007; 23:10603. [PubMed: 17803323]

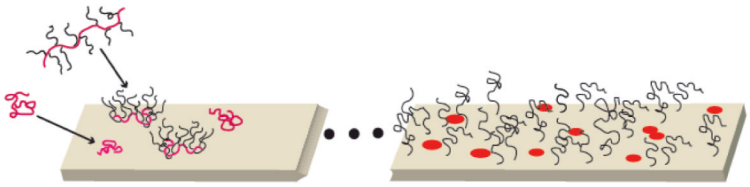

Figure 1.
Scheme of protocol for preparing patchy brush surfaces.

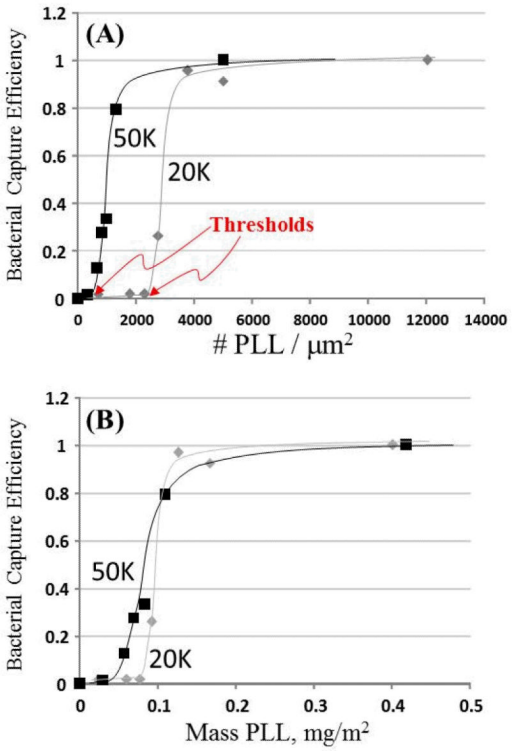

Figure 2.

The effect of the molecular weight of the PLL patches in Brush #2 on the bacterial capture efficiency, for 20,000 (gray diamonds) and 50,000 (black squares) PLL, plotted as a function of (A) patch number and (B) patch mass. The curves are drawn by eye. Data are for pH 7.4, Debye length κ^{-1} = 2 nm, wall shear rate γ = 5 s^{-1}. The nominal bacteria solution concentration is 5×10^5 / ml.

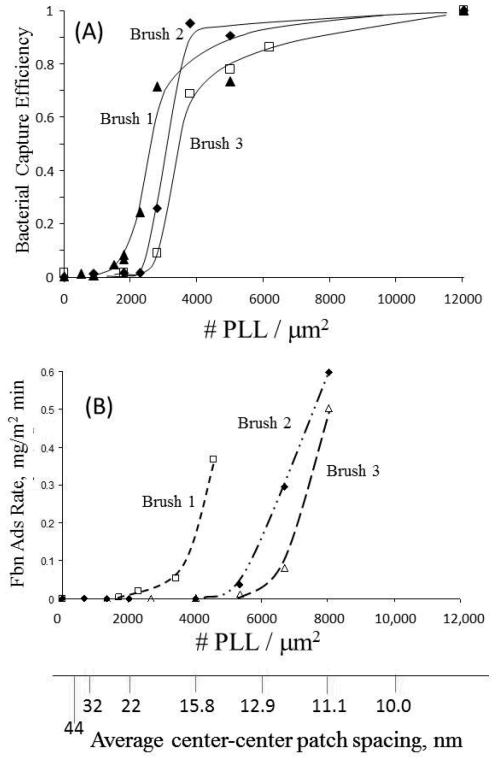

Figure 3.

A) Bacterial capture efficiencies on three different brushes containing embedded 20,000 molecular weight poly-l-lysine patches. Adsorption is from flow at $\gamma = 5\ s^{-1}$ and an ionic strength of 0.026 M corresponding to $\kappa^{-1} = 2$ nm. B) Fibrinogen adsorption on the same surfaces for $\kappa^{-1} = 2$ nm, from reference 32.

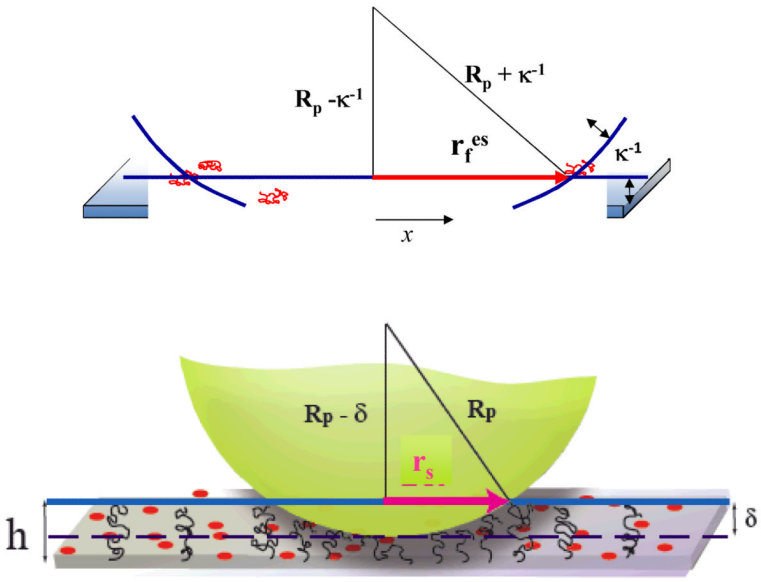

Figure 4.

Schematic of bacteria contact with a patchy brush surface. (A) defining the electrostatic interaction radius, r^{es}_f (B) defining the steric brushy interaction radius, r_s, for brush height h and brush compression δ. The final separation is h' = h -δ. The compression is large when h'/h < 0.25.

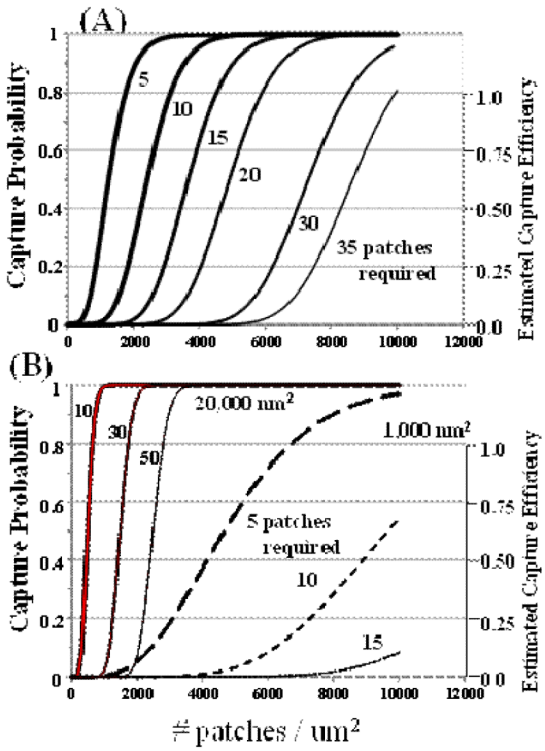

Figure 5.

Calculated capture efficiencies from the statistical model. (A) The effect of valency on capture efficiency and probability, for an electrostatic contact area of 4000 nm^2. (B) The influence of contact area on capture, over the range of valencies relevant to bacteria capture.

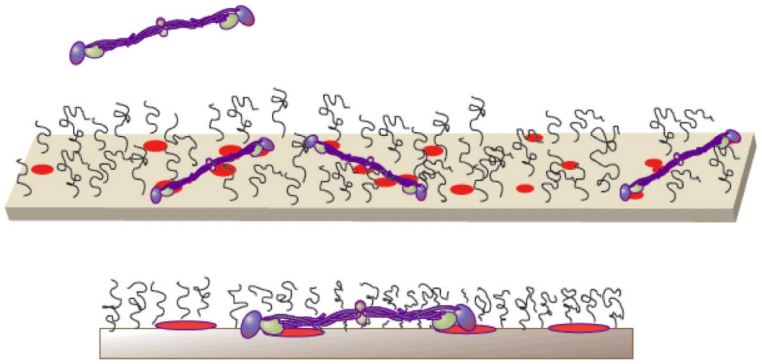

Figure 6.
Side on fibrinogen adsorption, required for bridging multiple patches, likely requires brush penetration, especially because the narrow fibrinogen dimension is smaller than the brush height.

Table I

Copolymer Samples

	Polymer I PLL-(2.7)PEG(2K)	Polymer II PLL-(2.2)PEG(5K)	Polymer III PLL-(4.7)PEG(5K)
PEG MW	2,000	5,000	5,000
Grating Ratio	2.7	2.24	4.5
% PLL	37%	45%	22%
Functionalization			
Molecular Weight	136,000	367,000	188,000

Table II

Brush Architectures

	Brush #1 PLL-(2.7) PEG(2K)	**Brush #2 PLL-(2.2) PEG(5K)**	**Brush #3 PLL-(4.7) PEG(5K)**
Saturated adsorption, mg/m^2	1.1	0.9	1.3
Adsorbed PEG, mg/m^2	**0.94**	**0.85**	**1.16**
Area /Copolymer, nm^2	206	680	247
Area /PEG tether, nm^2	3.6	9.6	7.2
Tether Spacing, $\sigma^{-1/2}$, nm *1	**1.9**	**3.1**	**2.7**
Number of Blobs	4.7	5.1	6.4
Brush Height, h_o, nm *2	**7.5 -9**	**14.5 - 15.5**	**16.5 - 17.2**

*1 Tether spacing is equivalent to the blob diameter, also called the brush persistence length; σ = areal density of tethers

*2 Brush heights show the range calculated for the Alexander-DeGennes treatment of the Flory brush and the semidilute brush of blobs. Calculations for both are detailed in the Supporting Information.

Table III

Brush Features Relevant to Steric Repulsion of Bacteria and Protein

	Brush 1	Brush 2	Brush 3
Calculated Bacterial Capture Valency for 20K PLL patch	13	18	20
Bacterial interaction radius,[1] r_s, nm	84	117	124
Bacterial interaction area, [1] nm^2	7,000	13,700	15,400
Fibrinogen interaction area, nm	150-200	150-200	150-200
PEG Content at Bacterial Threshold (20K patch), mg/m^2	0.81	0.80	1.11
Brush Height at Bacterial Threshold, nm (20K patch)	7	13	16
Brush Compression Energy, 2nd virial Relative to that of Brush 1 [2]	---	0.98	1.88
Brush Compression Energy, full osmotic expression, relative to Brush 1	---	0.9	2.9
PEG Content at Fibrinogen Threshold,[32] mg/m^2 (20K patch)	0.57 ±0.12	0.6 ±0.04	0.80 ±0.13
Brush Height at Fibrinogen Threshold, nm (20K patch)	6	12	14
Average Tether Spacing at Fibrinogen Threshold, nm (20K patch), $\sigma^{-1/2}$	2.4±0.2	3.7±0.1	3.2±0.3
Steric (Penetration) Repulsion, kT per Fibrinogen	180	50	65
StericCompression Penalty, kT per Fibrinogen	68	20	25

[1] Assumes an ultimate gap separation of 2 nm

[2] Assumes similar brush compressions for all brushes